

The HI Dominated Low Surface Brightness Galaxy KKR17

M. I. Lam^{1,2,3*}, H. Wu^{1,3†}, M. Yang^{1,3}, Z. -M. Zhou^{1,3}, W. Du^{1,3}, and Y. -N. Zhu^{1,3}

¹ National Astronomical Observatories, Chinese Academy of Sciences, Beijing, 100012, China

² University of Chinese Academy of Sciences, Beijing, 100049, China

³ Key Laboratory of Optical Astronomy, National Astronomical Observatories, Chinese Academy of Sciences

Received 2014 August; in original form 2014 August

ABSTRACT

We present new narrow-band ($H\alpha$ and [OIII]) imagings and optical spectrophotometry of HII regions for a gas-rich low surface brightness irregular galaxy, KKR 17. The central surface brightness of the galaxy is $\mu_0(B) = 24.15 \pm 0.03$ mag sec⁻². The galaxy was detected by *Arecibo Legacy Fast ALFA survey* (ALFALFA), and its mass is dominated by neutral hydrogen (HI) gas. In contrast, both the stellar masses of the bright HII and diffuse stellar regions are small. In addition, the fit to the spectral energy distribution to each region shows the stellar populations of HII and diffuse regions are different. The bright HII region contains a large fraction of O-type stars, revealing the recent strong star formation, whereas the diffuse region is dominated by median age stars, which has a typical age of ~ 600 Myrs. Using the McGaugh's abundance model, we found that the average metallicity of KKR 17 is $12 + (O/H) = 8.0 \pm 0.1$. The star formation rate of KKR 17 is 0.21 ± 0.04 M_⊙/yr, which is $\sim 1/5$ of our Milky Way's. Based on the analysis results to young stellar clusters in HII region, it is found that the bright HII region showed two sub-components with different velocities and metallicities. This may be caused by the outflow of massive stars or merging events. However, the mechanism of triggering star formation in the HII region is still uncertain.

Key words: galaxies: abundances — galaxies: evolution — galaxies: individual (KKR 17) — galaxies: irregular

1 INTRODUCTION

Low surface brightness galaxies (LSBGs) are thought to be important baryonic contributor to the universe (see Impey & Bothun 1997; Bothun, Impey & McGaugh 1997 for a review). The initial study by Freeman (1970), based on spiral galaxies, found that the central surface brightness of disk galaxies was concentrated on a very narrow range. Subsequently, Disney (1976) pointed out the surface brightness resulted from Freeman (1970) may be due to the selection effect and predicted the existence of galaxies fainter than sky background. Indeed, many surveys later have discovered a large number of LSBGs (e.g. Schombert & Bothun 1988; Schombert et al. 1992; Bothun et al. 1992; Caldwell & Bothun 1987; Impey et al. 1996). They span a very wide range in morphology (ranging from dwarfs and irregulars to giant disk galaxies), stellar mass and colors ($0.3 < B-V < 1.7$) (e.g. McGaugh, Schombert, & Bothun 1995; O'Neil et al. 1997). Considering their metal content, most LSBGs present low

metallicity (see, e.g. Skillman, Kennicutt & Hodge 1989a; Skillman, Terlevich & Melnick 1989b), although the metallicities of some red LSBGs have been found to be around the solar metallicity (Bergmann et al. 2003).

Star formation plays a crucial role in the evolution of LSBGs. Usually, star formation in galaxies could be divided into four different kinds of mode: (1) instantaneous star formation, typically in interaction/merging event, (2) normal star formation with relatively higher star formation rate (SFR; about $1\sim 5$ M_⊙/yr), typically in normal spiral galaxies under gravitational wave density, (3) continuous star formation under very low SFR in long time-scale, typically in dwarf galaxies (Schombert, Maciel & McGaugh 2011) and (4) episodic (sporadic) star formation, star formation do not need to be a continuous process under small fluctuation, typically in LSBGs (McGaugh 1994). LSBGs are found to have relatively low SFRs, probably an order of magnitude lower than HSBGs (Bothun, Impey & McGaugh 1997; Kim 2007). Previous studies showed that the evolution of LSBGs was much slower than that of their high surface brightness counterparts (HSBGs), and most of their stellar mass was formed by the third star formation mode. However, Schombert, McGaugh & Eder (2001) argued that the weak

* Email: linminyi@nao.cas.cn

† Email: hwu@bao.ac.cn

bursts/interaction may still occur in LSBGs in the recent 5 Gyrs. Kim (2007) found that the LSBGs may experience episodic star formation activities along Hubble time due to gas infalling. Recently, Schombert, McGaugh & Maciel (2013) and Schombert & McGaugh (2014) both found the star formation mechanism in their sample appeared to be the same as those of HSBGs, and the total stellar mass formation in LSBGs were close to a Hubble time, alternatively, it was a normal star formation mode. All of these results reveal that the star formation activities in LSBGs are still controversial.

In order to better understand the effects on evolution of LSBGs, it is essential to study the star formation properties of nearby LSBGs. Therefore, we selected one typical blue LSBG from Arecibo Legacy Fast ALFA Survey (ALFALFA; Giovanelli et al. 2005a), KKR 17, to investigate its possible star formation activity. KKR 17 has one bright, compact knot, and one extended, faint diffuse region. This galaxy was firstly discovered by the Second Palomar Sky Survey (POSS-II) films (Karachentseva, Karachentsev & Richter 1999), and its redshift was confirmed to be 0.0276 (Makarov, Karachentsev & Burenkov 2003). In addition, its HI flux was measured by using the 100-m radio telescope at Effelsberg (Huchtmeier, Karachentsev & Karachentseva 2000). The Arecibo ALFALFA survey showed its gas mass was quite high. Based on literature available, KKR 17 is still poorly studied and could be an ideal laboratory to test some of the star formation models.

In this paper, we explored the global properties of KKR 17, using the multi-wavelength observations from ultraviolet (UV) to near-infrared (NIR), and mainly focusing on the star formation and stellar population. The observations and relevant data reduction are presented in §2. The main results of our analysis are presented in §3. Discussions and summary are presented in §4 and §5, respectively.

2 OBSERVATION AND DATA REDUCTION

We used the archived far-UV (FUV), Near-UV (NUV) images from *Galaxy Evolution Explorer* (GALEX), optical wide-band images (*ugriz*) from *Sloan Digital Sky Survey* (SDSS), mid-infrared 3.4 μm images from *Wide-Field Infrared Survey Explorer* (WISE) and HI data from *Arecibo Legacy Fast ALFA Survey* (ALFALFA). In addition, we have obtained optical narrow-band images and spectra of KKR 17 by using BAO Faint Object Spectrograph and Camera (BFOSC) mounted on 2.16m telescope at Xinglong Observatory, National Astronomical Observatories of Chinese Academy of Science (NAOC). Detailed information is given in Table 1.

2.1 Ultraviolet Images

The GALEX mission was launched in 2003, and it has surveyed all sky simultaneously in two broad-bands. The effective wavelength of FUV instrument is 1516Å, and NUV is 2267Å (Martin et al. 2005). The field of view (FOV) of GALEX is $\sim 1.2^\circ$ (Morrissey et al. 2007). We obtained the images from GALEX Medium Imaging Survey (MIS; $\sim 1500\text{s}$), which was designed to cover 1000 deg² and reach

to $m_{AB} \approx 23$ mag. This survey could also cover the maximum area of SDSS survey. The keywords of mean sky-background level (SKY) and AB magnitude zero point (ZP) in the header of image were used for sky subtraction and flux calibration, respectively. The final image has a spatial resolution of 6'' and a pixel size of 1.5''.

2.2 Optical images

The optical broadband images (*ugriz*) were taken from SDSS data archive server (York et al. 2000; Stoughton et al. 2000). The background was subtracted from each image before photometry, and the counts were converted to flux densities and magnitudes.

The new images with narrow-band filters (centered at redshifted H α and [OIII], respectively) and broad-band filters (V- and R-bands) were observed with BFOSC on 2.16m telescope at Xinglong Observatory, NAOC on June 16 2012. The FOV of BFOSC is approximately 8.5' \times 9.5', with the CCD size of 1130 \times 1230 pixels. One pixel of BFOSC corresponds to $\sim 0.45''$. The continuum-subtracted [OIII] images included both [OIII] $\lambda\lambda$ 4959 and 5007 in our images. However, The continuum-subtracted 'H α ' images still included a component from [NII] $\lambda\lambda$ 6548,6583 emission lines. Fortunately, the doublet [NII] lines were very weak in the low metallicity environment, which could contaminate $\sim 5\%$ fluxes at most to our narrow-band image and is much less the flux calibration error. Therefore, we neglected the [NII] emission lines in KKR 17 in our analysis.

All standard CCD reductions were performed before astrometric and flux calibrations. The SDSS field stars were used as references for astrometric and flux calibration, and the astrometric calibration accuracy is better than 1'' in our images. Flux calibrations were converted between SDSS and UBVR_cI_c magnitude systems, using the conversion coefficients in Lupton(2005)¹. The V- and R-band images were used as stellar continuum, which would be subtracted from narrow-band [OIII] and H α images. We estimated that the error of integrated flux is less than 20% in the narrow-band images, which was limited by the low surface brightness of the galaxy and the flux calibration error.

2.3 Infrared Data

The infrared images of KKR 17 were taken from WISE satellite (Wright et al. 2010). The mission was launched in 2009 and began to survey all sky in 2010. The astrometric accuracy for high signal-to-noise (S/N) images was better than 1.5''. The angular resolution was 6.1'', 6.4'', 6.5'' and 12.0'' at the wavelengths of 3.4, 4.6, 12 and 22 μm , respectively. KKR 17 was only found at 3.4 μm due to the contamination of nearby bright stars. Moreover, as shown in Figure 1, 3.4 μm is also contaminated by the nearby bright stars. Therefore, we need to mask the bright star to perform the aperture photometry in this band.

¹ <http://www.sdss.org/dr7/algorithms/sdssUBVRITransform.html>

Table 1. Observation Log

| Band | Telescope | Instrument | λ_{eff} (μm) | Exposure Time (sec) | Date (UT) | FWHM ($''$) | Pixel Size ($'' \text{ pixel}^{-1}$) |
|-------------------|-----------|------------|--------------------------------------|------------------------|--------------|------------------|---|
| FUV | GALEX | ... | 0.1516 | 1701.05 | 2009 May 28 | 6.0 | 1.500 |
| NUV | GALEX | ... | 0.2267 | 1701.05 | 2009 May 28 | 6.0 | 1.500 |
| <i>u</i> | SDSS | ... | 0.3543 | 53.9 | 2003 Jun 22 | 1.4 | 0.396 |
| <i>g</i> | SDSS | ... | 0.4770 | 53.9 | 2003 Jun 22 | 1.4 | 0.396 |
| <i>r</i> | SDSS | ... | 0.6231 | 53.9 | 2003 Jun 22 | 1.4 | 0.396 |
| <i>i</i> | SDSS | ... | 0.7625 | 53.9 | 2003 Jun 22 | 1.4 | 0.396 |
| <i>z</i> | SDSS | ... | 0.9134 | 53.9 | 2003 Jun 22 | 1.4 | 0.396 |
| 3.4 μm | WISE | ... | 3.368 | ... | 2010 | 6.0 | 1.375 |
| 21 cm | Arecibo | L-band | 21 cm | ... | ... | $\sim 3.5'$ | ... |

| Our Observations | | | | | | | |
|------------------|----------------|-------|------------|-----------------|-------------|-----|------|
| V | Xinglong 2.16m | BFOCS | 0.545 | 2×300 | 2012 Jun 16 | 2.2 | 0.45 |
| R | Xinglong 2.16m | BFOCS | 0.700 | 2×300 | 2012 Jun 17 | 2.2 | 0.45 |
| [OIII]-4 | Xinglong 2.16m | BFOCS | 0.516 | 2×1800 | 2012 Jun 16 | 2.2 | 0.45 |
| H α -5 | Xinglong 2.16m | BFOCS | 0.676 | 3600 | 2012 Jun 17 | 2.2 | 0.45 |
| Spectrum (G6) | Xinglong 2.16m | BFOCS | 0.33-0.545 | 3600 | 2013 Mar 10 | 3.0 | 0.45 |
| Spectrum (G7) | Xinglong 2.16m | BFOCS | 0.39-0.67 | 3600 | 2013 Jun 15 | 1.8 | 0.45 |
| Spectrum (G8) | Xinglong 2.16m | BFOCS | 0.58-0.82 | 3600 | 2012 Jun 17 | 2.2 | 0.45 |

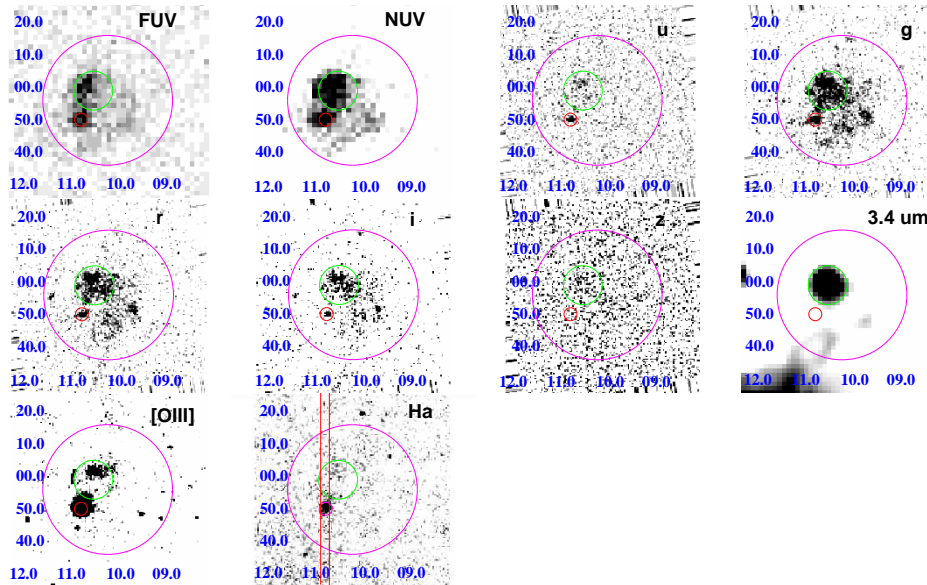


Figure 1. The multi-wavelength images of KKR 17 (centered on RA = 15:11:10.2 & DEC = +11:01:56). From left to right and from top to bottom are FUV, NUV images from GALEX, *ugriz* images from SDSS, 3.4 μm image from WISE and [OIII], H α narrow-band images from 2.16m telescope at Xinglong observatory. The narrow-band images were already stellar-continuum subtracted. The magenta circles are our aperture circle. The spectra was extracted from region 1 (red circles), the low mass stars are dominated in region 2 (green circles). The red lines in H α image indicate the position of long-slit of our spectrum.

2.4 HI Data

The *Arecibo Legacy Fast ALFA survey* (ALFALFA; Giovanelli et al. 2005a) is the largest blind HI line survey nowadays. The current catalog, ‘ $\alpha.40$ ’, which covered $\sim 40\%$ of the final targeted sky area (Haynes et al. 2011), contained $\sim 15,000$ extragalactic sources in the regions of (1) spring: $07^h 30^m < \text{RA} < 16^h 30^m$, $+04^\circ < \text{DEC} < +16^\circ$ and $+24^\circ$

$< \text{DEC} < +28^\circ$, and (2) fall: $22^h < \text{RA} < 03^h$, $+14^\circ < \text{DEC} < +16^\circ$ and $+24^\circ < \text{DEC} < +32^\circ$. The catalog includes the source information on position, HI fluxes, HI masses, systemic velocities, and HI line width, etc.

The 21 cm line profile of KKR 17 is archived from ALFALFA survey (Giovanelli et al. 2005a). The HI line of KKR 17 is shown as a single-horn profile on the velocity map, which may indicate that it is a face-on or unstable-

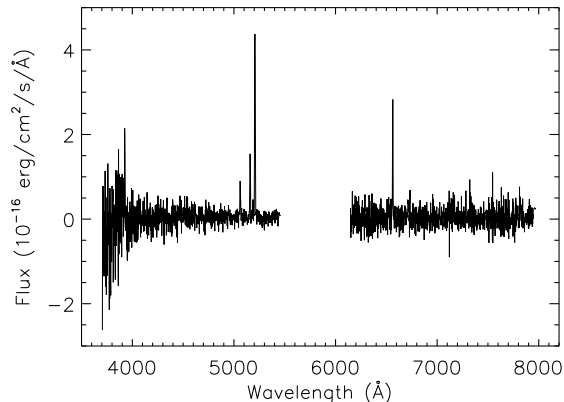


Figure 2. The spectra of HII region (region 1 in Figure 1) of KKR 17.

disk galaxy. The HI mass of KKR 17 is $\sim 4.37 \times 10^9 M_{\odot}$ in 120.8 Mpc (Haynes et al. 2011), which shows the mass of neutral hydrogen is comparable to that in a normal galaxy. The receding velocity of the galaxy is 8283 ± 4 km/s, which is consistent with the Hubble flow velocity inferred from the redshift ($z=0.0277$) of our spectral analysis.

2.5 Photometry

Photometries of data in all bands were performed after CCD pre-procedures, which included overscan subtraction, bias subtraction, flat-field correction, cosmic-ray reduction and background subtraction. The IRAF task SURFIT was used for background subtraction. We used the IRAF task PHOT to produce the photometry with the same aperture, and fixed the aperture center at RA = 15:11:10.2, DEC = +11:01:56. The aperture radius was $20''$ for entire analysis. In addition, we selected two different regions to analyze their properties: (1) the ‘diffuse’ region centered on RA = 15:11:10.5, DEC = +11:01:59 with photometric aperture radius of $6''$; (2) the HII region centered on RA = 15:11:10.76, DEC = +11:01:50.05, with photometric aperture radius of $2''$. All the photometric results are shown in Table 2.

2.6 Optical Spectra

The optical spectra of the HII region in KKR 17 were observed on March 10, 2013 (G6+ $1.8''$), June 15, 2012 (G7+ $1.8''$) and June 17, 2012 (G8+ $1.8''$). The observations were also performed by BFOSC on 2.16m telescope. A slit with a width of $1.8''$, combining with three different grisms (G6 from 3600 to 5450Å, G7 from 4000 to 6700Å, and G8 from 5800 to 8000Å), were used for the observation. However, only G6 and G8 spectra were analyzed. The resolution of the grism is $\sim 10\text{Å}$. KKR 17 and its HII regions cannot be seen by the guide cameras of 2.16 telescope because their flux is quite low. So it is kind of tricky to put the slit properly. We noticed that there was one bright star nearby in the field of view of guide camera, and we estimated the offset between the star and HII region through the narrow-band image. The slit was then fixed at the position with the estimated offset relative to the star. The CCD reductions including overscan

Table 3. Emission-Lines Fluxes and Errors

| Line | Equivalent Width (EW) (Å) | Intensity (I_{λ}) (10^{-15} erg/s/cm 2) |
|-----------------------|------------------------------|---|
| 2012 Jun 15 | | |
| upper aperture | | |
| H β (4861Å) | -249.5 ± 23 | 1.25 ± 0.10 |
| [OIII] λ 4959 | -667.5 ± 32 | 1.82 ± 0.09 |
| [OIII] λ 5007 | -2429 ± 645 | 5.13 ± 0.10 |
| bottom aperture | | |
| H β (4861Å) | -552.3 ± 188 | 0.46 ± 0.10 |
| [OIII] λ 4959 | -427.9 ± 50 | 0.68 ± 0.08 |
| [OIII] λ 5007 | -3537 ± 278 | 1.62 ± 0.09 |
| 2012 Jun 17 | | |
| H α (6563Å) * | -593.6 ± 33 | 1.81 ± 0.13 |
| [NII] λ 6583 | -27.6 ± 36 | 0.10 ± 0.10 |
| 2013 Mar 10 | | |
| [OII] λ 3727 | -225.9 ± 11 | 1.59 ± 0.11 |
| H β (4861Å) * | -212.2 ± 72 | 0.80 ± 0.10 |
| [OIII] λ 4959 | -290.1 ± 40 | 1.23 ± 0.10 |
| [OIII] λ 5007 | -610.7 ± 16 | 3.85 ± 0.09 |

*: The high $I(\text{H}\beta)/I(\text{H}\alpha)$ ratio of KKR 17 is due to double-components of H β emission line. The spectra resolution was limited by the telescope aperture, and it is a small-size telescope in our case. The spectral resolution for 2.16m telescope is only $\sim 10\text{Å}$, which is challenging to distinguish the precise sub-structures of KKR 17. Also, the observation seeings on two days were different, which may lead to a small position deviation between two spectra.

and bias subtraction, flat-field correction and cosmic-ray reduction were performed before wavelength and flux calibrations. The Fe/Ar lamp was used as the wavelength standard in our spectra, and the Kitt Peak National Observatory IRS standard stars were adopted as flux standard. The optical spectra were shown in Figure 2 and all strong emission lines that we measured were shown in Table 3.

3 RESULTS

3.1 Multiwavelength Morphologies in KKR 17

KKR 17 is an irregular, gas-rich galaxy. It shows a significant bright HII region and a very diffuse, faint region. Figure 1 showed the different band images from FUV to NIR and the continuum-subtracted [OIII] and H α images. We separated KKR 17 into two different parts, and discussed their different spectral energy distributions (SEDs) and stellar populations in the following sections. KKR 17 showed different morphologies from UV to NIR, and also centered on different regions in different bands. The HII was the brightest

Table 2. Properties of KKR 17

| Parameter | Diffuse region | HII region | Total |
|--|----------------|--------------|------------------------|
| Optical RA (J2000) | 15:11:10.5 | 15:11:10.76 | 15:11:10.2 |
| Optical Dec (J2000) | +11:01:59 | +11:01:50.05 | +11:01:56 |
| Radio RA (J2000) | ... | ... | 15:11:07.90 |
| Radio Dec (J2000) | ... | ... | +11:02:37 |
| W50 ^a | ... | ... | 29 ± 2 |
| F _{HI} ^b | ... | ... | 1.26 ± 0.05 |
| Distance ^c | ... | ... | 120.8 ± 8.5 |
| M _{HI} /M _⊙ ^d | ... | ... | 4.37 × 10 ⁹ |
| μ ₀ (B) ^e | ... | ... | 24.15 ± 0.03 |
| FUV ^f | 23.29±0.19 | 21.44±0.10 | 19.09±0.06 |
| NUV | 20.14±0.08 | 21.64±0.06 | 19.02±0.04 |
| <i>u</i> ^g | 19.54±0.10 | 20.60±0.12 | 18.43±0.15 |
| <i>g</i> | 18.72±0.02 | 20.22±0.04 | 17.68±0.03 |
| <i>r</i> | 18.62±0.03 | 20.49±0.07 | 17.49±0.04 |
| <i>i</i> | 18.48±0.04 | 20.93±0.14 | 17.37±0.06 |
| <i>z</i> | 18.46±0.15 | 20.88±0.44 | 17.18±0.22 |
| [OIII] ^h | 0.78±0.08 | 1.26±0.03 | 1.86±0.20 |
| Hα | 0.33±0.08 | 0.64±0.03 | 1.51±0.26 |
| 3.4 μm | 19.98±0.21 | 22.76±0.59 | 18.78±0.15 |

(a) The unit of W50: km s⁻¹; (b) unit of F_{HI}: Jy km s⁻¹; (c) unit of distance: Mpc; (d) calculate the mass with the distance of 120.8 Mpc; (e) unit of μ₀(B): (magsec⁻²); (f) unit of FUV, NUV and 3.4μm: mag in AB system; (g) unit of *ugriz*: mag in SDSS system; (h) unit of [OIII] and Hα: 10⁻¹⁴ erg/s/cm².

region in FUV and NUV, in contrast, the diffuse region was also bright in NUV, but faint in FUV. In addition, in the optical *u* band which has a low sensitivity, HII and diffuse regions showed different features: the diffuse region was barely detectable, but HII region was still bright enough for detection. The optical *g*-, *r*-, *i*-band images showed very similar morphologies for KKR 17. This galaxy showed an unstable-disk feature in *g*-, *r*-, and *i*-bands. However, *g*- and *r*-band images are contaminated by the [OIII] and Hα emission, respectively. The narrow-band [OIII] image with continuum subtracted showed the emission in the bright HII knot was relatively stronger than the one in the diffuse region, although the radiation fields in both bright HII knot and diffuse region were strong. However, only the narrow-band Hα image showed the bright HII region, which indicates HII knot are undergoing relatively strong star formation activity. The low sensitivity optical *z*-band image was faint in both two regions. The 3.4 μm emission is dominated by the ones from late-type stars centered at RA = 15:11:10.5, DEC = +11:01:59, which may be the real galactic center. The disappearance of HII region in 3.4 μm also revealed that the mass of this region was relatively small.

3.2 Surface Brightness

To obtain the surface brightness (SB) profile of KKR 17, we first adopted a geometric center from NED and decomposed the galaxy structure using GALFIT (Peng et al. 2002). Since KKR 17 was bulgeless (Sérsic index < 1), we fitted the galaxy with the single exponential profile. We obtained the semi-axis ratio of b/a = 0.92, the inclination angle of 34.90 degree and the disk scale length of $r_s = 7.52$ arcsec. The galactic scale length is equivalent to the linear scale length of 4.20 kpc at this redshift, which was comparable

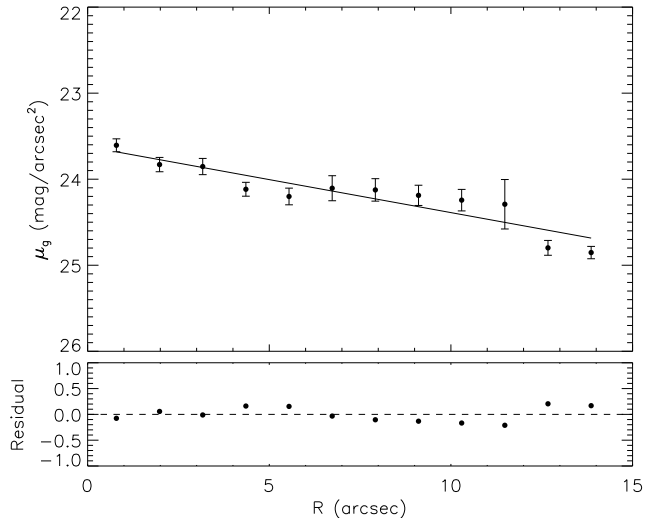


Figure 3. The surface brightness profile of KKR 17. The solid line shows the best-fitted single exponential component was shown in solid line. The best-fit is consistent with the outer region of galaxy and GALFIT decomposition results.

to nearby giant LSBG Malin 1 (Barth et al. 2007). Then, we performed the concentric elliptical aperture photometry according to the GALFIT's results. The surface brightness profile of KKR 17 in the *g*-band was shown in Figure 3 and the color of *g* - *r* was ~ 0.15 mag. The best-fitted single exponential profile indicated that KKR 17 was a bulgeless galaxy.

In order to obtain the central surface brightness, we

converted the SDSS magnitude to Johnson B-band magnitude (Lupton 2005). Then we use the following relation from Galaz et al. (2011) to calculate the surface brightness of KKR 17:

$$\mu_0(B) = B + 2.5 \log(2\pi a^2) + 2.5 \log(b/a) - 10 \log(1+z) \quad (1)$$

The values of the semi-axis ratio and redshift are taken from the GALFIT results, and the central surface brightness of KKR 17 was found to be $\mu_0(B) = 24.14 \pm 0.03 \text{ mag sec}^{-2}$.

3.3 Stellar Population

The color of a galaxy could reveal its star formation history (SFH), since the older stellar population would have the redder color, and the younger stellar population would have a bluer color. Previous study found the ages of blue LSBGs span a wide range, from young (2 Gyr) (Zackrisson et al. 2005) to old (~ 7 Gyr) (Jimenez et al. 1998), which depends on the physical conditions both in the disk and SFR (Vorobyov et al. 2009). One of the explanations for these blue LSBGs was that they may be formed by the episodic star formation process (e.g. McGaugh 1994; Gerritsen & de Blok 1999; Bothun, Impey & McGaugh 1997). The episodic star formation process means the stars could form through a discrete process in small perturbation. The star formation process could carry out both active and quiescent periods in the galaxy and last in a few Gyrs. The global stellar population was contributed by the low SFR, and the bright HII region was formed by the episodic star formation process. KKR 17 is classified as very blue LSBG, based on the definition of O’Neil et al. (1997) (U-B and B-V colors of KKR 17 were 0.25 and 0.27, respectively). It had a significant bright HII region but a faint, diffuse region, which would be a perfect testbed for the theoretical models of LSBGs.

The FUV-to-optical SED of the total, diffuse region, and HII knot of KKR 17 were shown in Figure 4. We compared the SEDs of KKR 17 with the different morphological templates to reveal the stellar population. We adopted the SED templates of elliptical, late-type spiral galaxies, and low dust extinction starburst galaxies (Reddening E(B-V) < 0.1) from Kinney et al. (1996), and also took one spectrum of typical low surface brightness galaxy UGCA357 (van Zee, Haynes & Salzer 1997). We normalized all fluxes of templates and KKR 17 in the central wavelength of i-band filter, which can avoid the strong emission of [OIII] and H α . The total continuum of KKR 17 seemed to be flatter compared to the ones of late-types and starbursts, and also revealed a hybrid stellar population, which could be the population combination of the spiral Sc galaxies and ellipticals. The HII knot was a typical young-star-dominated region. However, the stellar populations of diffuse region was quite different from that of HII knot. The diffuse region showed a flux jump between NUV and FUV, which is a typical spectral feature for A-type stars (Gulati et al. 1994). Thus the diffuse region may be dominated by A-type stars. Hence, the diffuse region is the most contributor to the mass of the galaxy, which was consistent with NIR 3.4 μm image.

To derive the visible stellar population in a more precise way, we adopted the stellar evolutionary tracks for single stellar population (SSP) with Salpeter IMF (Salpeter 1955). The stellar evolution tracks were calculated based on

Charlot & Bruzual (CB2007) SSP models under the instantaneous SF law, which were effective to the episodic star formation and instantaneous starburst. For KKR 17, the best metallicity O/H value was adopted to be $Z = 0.004$ (See §3.5). Figure 5 showed the *ugr* color-color diagram of the entire galaxy, HII region, and diffuse region. We considered both the cases with and without emission lines subtracted. The integrated (*u* - *g*), (*g* - *r*) colors of entire KKR 17 and diffuse region correspond to ages of ~ 600 Myr. In addition, the HII region is much younger than diffuse region, and the intergrated colors revealed that the age of stellar population of this region was ~ 40 Myr. However, the age of HII region was hard to be defined after emission lines was subtracted because the emission lines in HII region were strong. As a add, it was hard to detect the continuum in HII region.

The flux over the wavelength range of HII in both SED and stellar synthesis model was similar to the ones of OB stars clusters, which to some extent means the HII region was undergoing star formation. However, the existence of large fraction of medium age (~ 600 Myr) stars in diffuse region may also be seen as the hint of different star formation histories in two regions.

3.4 Stellar Mass

The stellar mass of galaxy is a crucial fundamental parameter for galaxy evolution. The mass-to-light ratio relation and single near-infrared luminosity can be used as useful estimators for the stellar masses. All the methods of constraining the stellar mass of galaxies suffers from a uncertainty of a factor of two because of large uncertainty in the contribution fraction by the thermally pulsing asymptotic branch (TP-AGB) stars in the stellar evolution model. The TP-AGB stars have been found to dominate at some evolutionary phases for galaxies (Bruzual 2007A). Many evolutionary tracks are biased when the TP-AGB contribution in stellar population synthesis models is considered. For example, the galaxy masses derived from Bruzual 2011 (hereafter CB11) and Bruzual 2007B (hereafter CB07) model are much lower than that derived from Bruzual & Charlot 2003 (hereafter BC03). In this paper, three different methods were adopted to check the consistency of the stellar mass of KKR 17.

1. Optical Mass-to-light Ratio: The mass-to-light ratio (M/L) can provide an effectively way to estimate stellar masses with small change from model to model. The value of the mass-to-light ratio properly falls within the reasonable range of IMF. Cole et al. (2001) and Bell et al. (2003) derived the M/L, and studied the stellar mass function by combining the near-infrared and optical photometries in normal-galaxies-dominated sample. de Blok, McGaugh & Rubin (2001) suggested the B-band stellar mass-to-light ratio (M/L_B) was around 1.4 for LSBGs. Under this assumption, the stellar mass was estimated based on the B-band absolute magnitude in Freeman (1970), and the obtained stellar mass for KKR 17 is $1.32 \times 10^9 M_\odot$ by using M/L_B .

2. Optical Colors: We also adopted the optical (*g* - *r*) color from Bell et al. (2003) to check the stellar mass derived from M/L_B . We used the following conversion:

$$\log \frac{M_\star}{M_\odot} = 0.4(M_{r,AB} - 4.67) + [a_r + b_r(g - r)_{AB} + 0.15] \quad (2)$$

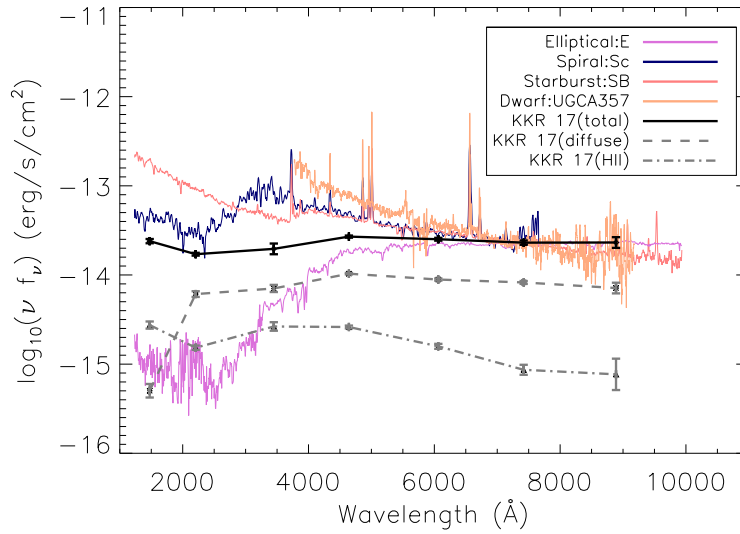


Figure 4. The spectral energy distributions of KKR 17, which included the global, diffuse and bright HII region. The templates of different type galaxies (E-Sc) are obtained from the Kinney-Calzetti Spectral Atlas of Galaxies (Kinney et al. 1996). The dwarf template is the spectrum of the typical LSBG UGCA357 (van Zee, Haynes & Salzer 1997). This figure shows that KKR 17 contains a large fraction of old stellar population, which is comparable to an elliptical galaxy, and the fraction of the young population, however, is lower than UGCA357, but comparable to a Sc-type spiral galaxy.

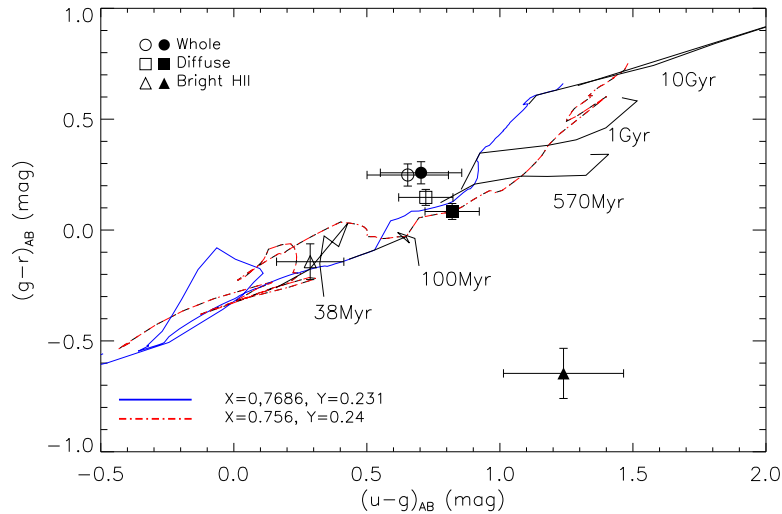


Figure 5. The ugr color-color diagram of the entire galaxy KKR 17 (*Circle*), HII region (*Square*) and diffuse region (*Triangle*) with error bar. *Open symbols*: the regions without emission lines ([OIII] & H α) subtracted, *solid symbols*: the regions with emission lines subtracted (more description see SS3.3). The stellar evolution tracks were using Charlot & Bruzual (CB07) SSP models under the instantaneous SF law. The stellar metallicity were adopted to $Z = 0.004$, which is the best model for the gas metallicity. *Blue solid line*: the stellar track with $X = 0.7686$ and $Y = 0.231$, *red dotted-dash line*: the stellar track with $X = 0.756$ and $Y = 0.24$, *Black solid lines*: the isochrone line of 38 Myr, 570 Myr and 10 Gyr, respectively.

where $M_{r,AB}$ was the r -band absolute magnitude, and $(g-r)_{AB}$ was the rest-frame color in the AB magnitude system. The coefficients a_r and b_r were adopted -0.306 and 1.097, respectively. The derived stellar mass of KKR 17 with the relation above was $1.22 \times 10^9 M_{\odot}$, which is close to previous method. As we can see, both results showed that the stellar mass of the galaxy was more than 2 times lower than its

mass of neutral hydrogen, which indicates that KKR 17 is dominated by neutral hydrogen. The gas fraction and gas ratio of KKR 17 are $f_{gas} \equiv \log(M_{gas}/(M_{\star} + M_{gas})) = -0.08$, and $\log(M_{gas}/M_{\star}) = 0.71$, respectively, which is a factor of 2 below the average gas fraction ($\log(M_{gas}/M_{\star}) \sim 1.5$) in 40% Arecibo ALFALFA total sample (Huang et al. 2012).

3. Monochromatic 3.4 μ m luminosity: The

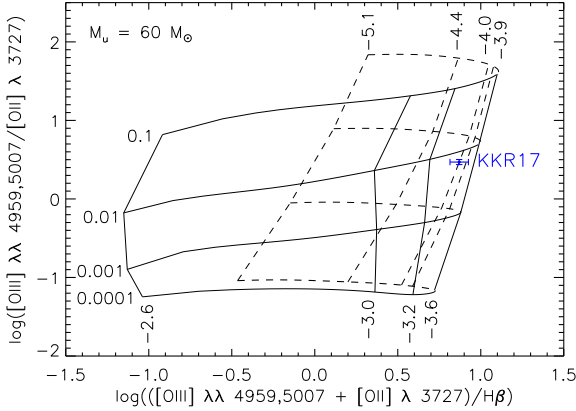


Figure 6. Diagnostic diagram of oxygen emission-line ratios compared with the photoionization models of McGaugh (1991). The position of KKR 17 indicates an oxygen abundance of $12 + \log(\text{O}/\text{H}) = 8.0 \pm 0.1$.

monochromatic $3.4\mu\text{m}$ luminosity is a convenient way to estimate stellar mass since it has a less dependence on star formation history and massive stars. Previous studies have found the $3.4\mu\text{m}$ luminosity could be a stellar mass tracer of galaxies (Wen et al. 2013), and we then used the following conversion method:

$$\log \frac{M_*}{M_\odot} = (-0.040 \pm 0.001) + (1.120 \pm 0.01) \times \log \left(\frac{\nu L_\nu(3.4\mu\text{m})}{L_\odot} \right) \quad (3)$$

The stellar mass of KKR 17 was $3.77 \times 10^8 M_\odot$, which is only one-third of the stellar mass derived from the M_B/L .

The stellar masses derived from the optical and near-infrared luminosity are quite different. The possible explanation was that the stellar mass estimate depended on TP-AGB model. The near-infrared luminosity in Method 3 may underestimate the stellar mass. In addition, considering Method 2 is less affected by the assumption compared to Method 1, and our adopted stellar mass of KKR 17 in this paper is $1.22 \times 10^9 M_\odot$.

3.5 Oxygen Abundance

Generally, LSBGs are found to be metal-poor ($Z < 1/3Z_\odot$) (McGaugh 1994). Some of them are the very metal-poor extragalactic objects discovered so far. The signal-to-noise ratio (S/N) of $[\text{OIII}]\lambda 4363$ of KKR 17 was not high enough, so we only calculated the oxygen abundance for the brightest HII region by using the strong-line method described in McGaugh (1991) (hereafter the McGaugh method) as following:

$$R_{23}: ([\text{OIII}]\lambda\lambda 4959, 5007 + [\text{OII}]\lambda 3727) / \text{H}\beta$$

$$O_{23}: ([\text{OIII}]\lambda\lambda 4959, 5007 / [\text{OII}]\lambda 3727)$$

Using the R_{23} and O_{23} values, the HII region of KKR 17 is overplotted on a grid of theoretical models and the abundance is determined by interpolating between the model points (see Figure 6). The models used for this work are from McGaugh (1991) in which the massive star produced from the IMF has a upper limit of $60M_\odot$.

The well-studied behavior of the strong oxygen lines (i.e., the R_{23} parameter) with different metallicity has been scaled to the oxygen abundance, using both empirical and theoretical methods (e.g. Edmunds & Pagel 1984; McGaugh 1991; Kewley & Dopita 2002; Nagao et al. 2006), which is the foundation of all these models. The ionization parameter can also be determined based on the additional parameter O_{23} which leads to a more accurate estimate of the abundance (e.g. Kewley & Dopita 2002; Nagao et al. 2006). However, the relationship between O_{23} and R_{23} is not unique: there exist two branches of models, (1) oxygen abundance decreases with an increase in R_{23} as ‘high-metallicity’ branch and (2) oxygen abundance increases with an increase in the R_{23} as ‘low-metallicity’ branch. In brief, each point on the grid of McGaugh’s models can lead to two different possible metallicity values.

In order to break the degeneracy, the $[\text{NII}]/[\text{OII}]$ ratio is used as a diagnostic to determine whether the HII region belongs to the ‘high-’ or ‘low-’ metallicity branch. For KKR 17, the HII region is located on the low-metallicity branch since $[\text{NII}]/[\text{OII}] < -1$. and the metallicity is $12 + \log(\text{O}/\text{H}) = 8.0 \pm 0.1$.

3.6 Star Formation Rates

Star formation rate (SFR) is an important parameter to describe the star formation activities as well as the evolutionary history of galaxies. SFR tracers are explored in a wide wavelength range from UV to sub-millimeter (e.g. Kennicutt (1998); Wu et al. (2005); Zhu et al. (2008); Calzetti et al. (2010)), especially in IR-band since it is closely related to HII region. KKR 17 is a typical low surface brightness galaxy, since the IR emissions was contaminated by the nearby bright stars. We adopted the narrow-band $\text{H}\alpha$ as the star formation tracer in this paper.

The total $\text{H}\alpha$ luminosity of KKR 17 was determined from the narrow-band image with both background and continuum subtracted, by integrating the flux over the aperture that encloses the entire galaxy. The total flux of $\text{H}\alpha$ we have obtained in KKR 17 was $(1.51 \pm 0.26) \times 10^{-14}$ erg/s/cm², or $L(\text{H}\alpha) = (2.65 \pm 0.46) \times 10^{40}$ erg/s for a distance of 120.8 ± 8.5 Mpc. In order to estimate the global SFR, we adopted the following relation Kennicutt (1998):

$$\text{SFR} (M_\odot/\text{yr}) = 7.9 \times 10^{-42} L(\text{H}\alpha) (\text{ergs/s}) \quad (4)$$

Then, it yields a total SFR of $0.21 \pm 0.04 M_\odot/\text{yr}$, and the specific star formation rate (sSFR) is $1.80 \times 10^{-10} \text{yr}^{-1}$, using the Bell et al. (2003)’s result, which means the time scale to form the total mass of KKR 17 under such SFR is 10^{10} yr. The sSFR value is slightly higher to the one for the typical E/S0 galaxies inferred for IR-selected sample Lam et al. (2013). Therefore, we conclude that the star formation process of KKR 17 is still in the episodic star formation process.

The flux coming from the HII region takes roughly 43% of total $\text{H}\alpha$ flux in the $\text{H}\alpha$ narrow-band image, which was consistent with the results of Schombert, McGaugh & Maciel (2013). The SFR in this HII region is $0.09 \pm 0.02 M_\odot/\text{yr}$, which is similar to the SFRs of young stellar clusters in M51 (Calzetti et al. 2005), a major merging system Arp 24 (Cao & Wu 2007), and a minor merger galaxy NGC7479 (Zhou et al. 2011).

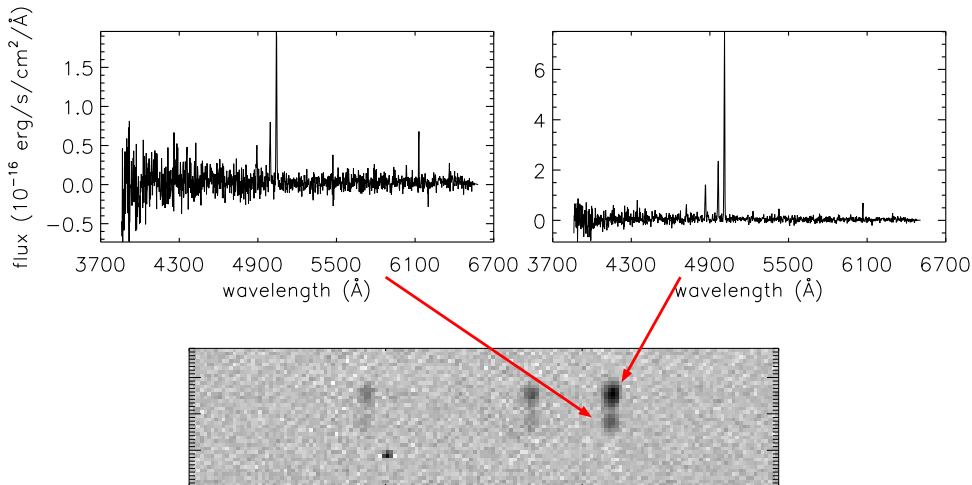


Figure 7. The substructure spectra of HII region. Left: bottom aperture ; right: upper aperture. The $H\beta$ and $[OIII]\lambda\lambda 4959,5007$ had slightly different velocities in two regions. Also, the ratios of $[OIII]\lambda\lambda 4959,5007$ in two regions were slightly different. The flux units were $\text{erg/s/cm}^2/\text{\AA}$ in the spectra.

4 DISCUSSION

4.1 Bright HII region

KKR 17 showed a clearly bright HII region, on its east side, dominated by the massive O stars. The HII region of KKR 17 was more compact and luminous than the Schombert, McGaugh & Maciel (2013)’s sample. The total $H\alpha$ luminosity of this HII region was approximately to $\log L(\text{HII}) = 40.06$ erg/s , within the radius of ~ 1 kpc. If the luminosity of a single O7V star in a HII region is $\log L(\text{HII}) = 37.0$ (Schombert, McGaugh & Maciel 2013; Werk et al. 2008), then thousands of O stars may exist in the HII region, and they contributed $\sim 50\%$ to $H\alpha$ luminosity in KKR 17, which is consistent with the previous results van Zee (2000) and Schombert, McGaugh & Maciel (2013).

The emission lines of HII region in KKR 17 showed the star formation processes may be complicated. Figure 7 showed two components in the same region of KKR 17. The physical separation of the two components was ~ 1.8 kpc, which similar to the size of the HII region. The components showed a small velocity difference of ~ 60 km/s identified by $[OIII]$ emission lines, and ~ 90 km/s by $H\beta$ emission line. Also, the metallicities were slightly different in terms of R_3 index, which can be easily obtained as a rough metallicity estimator but with relative large uncertainty. The parameter R_3 can be obtained through the simple relation of $R_3 = 1.35 \times I_{[OIII]5007}$ (Vacca & Conti 1992), where $I_{[OIII]5007}$ is the flux of $[OIII]$. Once the value of R_3 is known, the metallicity of $12 + \log (O/H)$ can be derived with the equation (7) in Vacca & Conti (1992). For the two flux values of $[OIII]$, which correspond to different components of HII region, the values of the metallicity are ~ 8.2 and ~ 8.3 , respectively,

and the difference is 0.1 dex. In contrast, it is noted that the systematic uncertainty is larger, 0.5 dex.

The small differences in the velocity and metallicity of HII components can be attributed to the internal episodic star formation activities. In fact, the young stellar clusters (YSCs), often found in HSBGs, can generate shocks, which can be used to explain those differences (Elmegreen 2004). Schombert, McGaugh & Maciel (2013) pointed out that the star formation processes in LSBGs are the same as the one in HSBGs. In addition, the recent research on YSCs in HSBGs found that YSCs are readily formed in a cluster complex than in an isolated environment (Bastian et al. 2005). The strong stellar wind from clustering massive stars could lead to those differences in YSCs. The shock-accelerated superwind was detected by nearby galaxies M82 and NGC839 (Rich et al. 2010). However, this was not supported by our spectra, we did not detect any line as the strong shock tracer, i.e., the $[SII]$ lines was weak and the $[NII]$ lines was an upper limit detection.

Another explanation is that each component had different origins. It was possible that the bright HII region was a dwarf galaxy fell into KKR 17 from a minor merger. The blue color of HII region, $g - i = -0.2$, is similar to the one for a irregular galaxy (Fukugita 1995), and its absolute magnitude ($M_B \sim -15$) resided at the faint end of luminosity function for the local extreme low-luminosity galaxies. Moreover, the unusual colors of $B - V = 0.27$ and $U - B = 0.21$ might also imply the existence of an infalling dwarf galaxy in KKR 17. The firm conclusion may still need a higher spatial resolution study for YSCs in KKR 17, e.g., the future IFU spectroscopy.

4.2 The Possible Evolution Scenarios of KKR 17

The LSBGs are usually thought to be evolving slowly across the Hubble time compared with their high surface brightness counterparts. The slow evolution may be connected with the small gas surface density (van der Hulst et al. 1993). If a LSBG is lack of neighbors over small and intermediate space scales, the absence of gravitational interaction will be able to keep the gas in a stable situation (Bothun et al. 1993). Also the other possibilities for the slow evolution of LSBGs could be due to the large dark matter halo, or low metallicity and dust content, or different IMF (Mihos et al. 1997; O’Neil et al. 1997).

The blue, gas-rich irregular galaxies, KKR 17, is located in Local Void in Hercules-Aquila direction. Theoretically, it may be far away from interaction in a long time scale, which leads to a low star formation rate. The previous studies on the SFH of IZw 18 showed that the continuously long-time low star formation activity can build up the stellar mass of galaxy (Aloisi et al. 1999; Legrand et al. 2000; Annibali et al. 2013). Although the slow star formation process can not be confirmed, we found that the KKR 17 experienced a short-duration star formation roughly 600 Myr ago. Kim (2007) pointed out the LSBGs were fast evolving in recent ~ 1 Gyr. Their results are in favor of the episodic star formation scenario (McGaugh 1992). The medium-age stellar population of diffuse region in KKR 17 may be dominant by A-type stars, which is consistent with the Kim (2007)’s result.

Except the star formation process occurred 600 Myr ago, the bright HII region is currently undergoing the strong star formation in KKR 17. The strong emission line features of HII region indicated the existence of a large fraction of O stars. The luminosity of HII region ($L(\text{H}\alpha) > 10^{40}$ erg/s) was unusually high to a LSBG (Helmboldt et al. 2009; Schombert, McGaugh & Maciel 2013). As suggested by Bastian et al. (2006), the star formation in such complicated YSC could be triggered by an external perturbation. If the perturbation was from an nearby galaxy, we should find the evidence in observations. However, we don’t found any objects from our FUV-to-NIR images. It is an isolated galaxy without any obvious large galaxies within a angular radius of $8'$, which is equivalent to ~ 250 kpc at its redshift. Based on the discussion above, the multiple components of H β and [OIII] emission lines may be a clue for the minor merger remnant, or the HII region was a dwarf galaxy, as discussed in Section §4.1, and experienced a minor merger. The deep interferometric imaging to KKR 17 with high spatial resolution and velocity dispersion may clean up the confusion, revealing its real star formation activity.

5 SUMMARY

In this paper, we present the results on metallicity and SFH of low surface brightness galaxy, KKR 17, with ground-based optical images and spectra combined with space telescope archival data, and they are summarized as the following:

1. KKR 17 is a HI-dominated low surface brightness galaxy of which the $M(\text{HI}) = 4.37 \times 10^9 M_{\odot}$, and the stellar mass is only about several $10^8 M_{\odot}$ to $10^9 M_{\odot}$ with a central surface brightness of $\mu_0(B) = 24.14 \pm 0.03$ magsec $^{-2}$.

2. The metallicity of the entire KKR 17 is $12 + \log(\text{O}/\text{H}) = 8.0 \pm 0.1$ with McGaugh (1991)’s model. However, the multiple components have a slightly different metallicities.

3. The global SFR of KKR 17 is $0.21 \pm 0.04 M_{\odot}/\text{yr}$, which is $\sim 1/5$ of our Milky Way’s. The sSFR is $1.80 \times 10^{-10} \text{ yr}^{-1}$ that leads to 10^{10} yr to form the total stellar mass of KKR 17. This sSFR was similar to the one for E/S0 galaxies. Therefore, KKR 17 is in quiescent star formation stage.

4. The fits to the optical SED and color-color diagrams of the diffuse and HII regions have revealed different stellar populations, which may represent the distinctive history of the star formation activities.

ACKNOWLEDGEMENTS

We would like to thank the staff of the 2.16m telescope at Xinglong Observatory for their excellent support during our observing runs. We would also like to thank Dr. L. J. Gou for his kindly help throughout the paper. We would like to acknowledge the anonymous referee for his/her helpful suggestions and comments.

This project is supported by the National Natural Science Foundation of China (Grant No.11173030), the China Ministry of Science and Technology under the State Key Development Program for Basic Research (2012CB821800, 2014CB845705), the National Natural Science Foundation of China (Grant Nos. 11225316, 11078017, 11303038, 10833006, 10978014, 10773014 and 11403061), the Key Laboratory of Optical Astronomy, the National Astronomical Observatories, Chinese Academy of Sciences. Supported by the Strategic Priority Research Program ‘The Emergence of Cosmological Structures’ of the Chinese Academy of Sciences, Grant No. XDB09000000.

We thank the work of the entire ALFALFA collaboration team in observing, flagging, and extracting the catalog of galaxies used in this work. We acknowledge NASA’s support for construction, operation, and science analysis for the *GALEX* mission.

Funding for the creation and distribution of the SDSS archive has been provided by the Alfred P. Sloan Foundation, the Participating Institutions, the National Aeronautics and Space Administration, the National Science Foundation, the U.S. Department of Energy, the Japanese Monbukagakusho, and the Max Planck Society. The SDSS website is <http://www.sdss.org>. The SDSS is managed by the Astrophysical Research Consortium (ARC) for the Participating Institutions.

This publication makes use of data products from the Wide-field Infrared Survey Explorer, which is a joint project of the University of California, Los Angeles, and the Jet Propulsion Laboratory/California Institute of Technology, funded the National Aeronautics and Space Administration.

REFERENCES

- Aloisi, A., Tosi, M., Greggio, L., 1999, *ApJ*, 118, 302
 Annibali, F., et al., 2013, *ApJ*, 146, 144
 Barth A. J., 2007, *AJ*, 133, 1085

- Bastian, N., Gieles, M., Efremov, Yu. N., Lamers, H. J. G. L. M., 2005, *A&A*, 443, 79
- Bastian, N., Emsellem, E., Kissler-Patig, M., Maraston, C., 2006, *A&A*, 445, 471
- Bergmann, M. P., Jørgensen, I., Hill, G. J., 2003, *AJ*, 125, 116
- Bell, E. F., McIntosh, D. H., Katz, N., Weinberg, M. D., 2003, *ApJS*, 149, 289
- Bothun, G. D., et al., 1992, *ApJ*, 395, 347
- Bothun, G. D., Schombert, J. M., Impey, C. D., Sprayberry, D., McGaugh, S. S., 1993, *AJ*, 106, 530
- Bothun, G., Impey, C., McGaugh, S., 1997, *PASP*, 109, 745
- Bruzual, G., Charlot, S. 2003, *MNRAS*, 344, 1000
- Bruzual, G., 2007, *ASPC*, 374, 303
- Bruzual, G. 2007, *IAUS*, 241, 125
- Bruzual, G. 2011, *RMxAC*, 40, 36
- Caldwell, N., Bothun, G. D., 1987, *AJ*, 94, 1126
- Calzetti, D., et. al., 2005, *ApJ*, 633, 871
- Calzetti, D., et al., 2010, *ApJ*, 714, 1256
- Cao, C., & Wu, H., 2007, *AJ*, 133, 1710
- Cole, S. et al., 2001, *MNRAS*, 326, 255
- de Blok, W. J. G., McGaugh, S. S., & Rubin, V. C., *AJ*, 2001, 122, 2396
- Disney, M.J., 1976, *Nature*, 263, 573
- Edmunds, M. G., & Pagel, B. E., 1984, *MNRAS*, 211, 507
- Elmegreen, B.G., 2004, *APSC*, 322, 277
- Freeman, K. C., 1970, *ApJ*, 160, 811
- Fukugita, M., Shimasaku, K., Ichikawa, T., 1995, *PASP*, 107, 945
- Galaz, G., Herrera-Camus, R., Garcia-Lambas, D., Padilla, N., 2011, *ApJ*, 728, 74
- Gerritsen, J. P. E., de Blok, W. J. G., 1999, *A&A*, 342, 655
- Giovanelli, R., et al. 2005, *AJ*, 130, 2598
- Gulati, R. K., Gupta, R., Gothoskar, P., Khobragade, S., VA, 38, 293
- Haynes, M. P., et al., 2011, *AJ*, 142, 170
- Huchtmeier, W. K., Karachentsev, I. D., Karachentseva, V. E., 2000, *A&AS*, 147, 187
- Huang, S. Haynes, M. P., Giovanelli, R., Brinchmann, J., 2012, *ApJ*, 756, 113
- Helmboldt, J. F., Walterbos, R. A. M., Bothun, G. D., O’Neil, K., Oey, M. S., 2009, *MNRAS*, 393, 478
- Impey, C. D., Sprayberry, D., Irwin, M. J., Bothun, G. D., 1996, *ApJS*, 105, 209
- Impey, C., Bothun, G., 1997, *ARAA*, 35, 267
- Jimenez, R., Padoan, P., Matteucci, F., Heavens, A. F. 1998, *MNRAS*, 299, 123
- Karachentseva, V. E., Karachentsev, I. D., & Richter, G. M., 1999, *A&AS*, 135, 221
- Kennicutt, R. C. Jr., 1998, *ARAA*, 36, 189
- Kewley, L. J., Dopita, M. A., 2002, *ApJS*, 142, 35
- Kim, J. H., 2007, Ph.D Thesis
- Kinney, A. L., et al., 1996, *ApJ*, 467, 38
- Lam, M. I., Wu, H., Zhu, Y.-N., Zhou, Z.-M., 2013, *RAA*, 13, 179
- Legrand, F., Kunth, D., Roy., J.-R., Mas-Hesse, J. M., & Walsh, J. R., 2000, *MNRAS*, 355, 891
- Makarov, D. I., Karachentsev, I. D., Burenkov, A. N., 2003, *A&A*, 405, 951
- Martin, D.C., et al., 2005, *ApJ*, 619, 1
- McGaugh, S. S., 1991, *ApJ*, 380, 140
- McGaugh, S. S., 1992, Ph.D Thesis
- McGaugh, S. S., 1994, *Nature*, 367, 538
- McGaugh, S. S., 1994, *ApJ*, 426, 135
- McGaugh, S. S., Schombert, J. M., Bothun, G. D. 1995, *AJ*, 109, 2019
- Mihos, J. C., McGaugh S. S., de Blok, W. J. G., 1997, *ApJ*, 481, 741
- Morrissey, P., et al., 2007, *ApJS*, 173, 682
- Nagao, T., Maiolino, R., & Marconi, A., 2006, *A&A*, 459, 85
- O’Neil, K., Bothun, G. D., Schombert, J., Cornell, M. E., Impey, C. D., 1997, *AJ*, 114, 2448
- Peng, C. Y., Ho, L. C., Impey, C. D.; Rix, H., 2002, *AJ*, 124, 266
- Rich, J. A., Dopita, M. A., Kewley, L. J., Rupke, D. S. N., 2010, *ApJ*, 721, 505
- Salpeter, E. E., 1955, *ApJ*, 121, 161
- Schombert, J. M., Bothun, G. D., 1988, *AJ*, 95, 1389
- Schombert, J. M., et al., 1992, *AJ*, 103, 1107
- Schombert, J. M., McGaugh, S. S., Eder., J., 2001, *AJ*, 121, 2420
- Schombert, J., Maciel, T., McGaugh, S., 2011, *AdAst*, 2011, 12
- Schombert, J. M., McGaugh, S. S., Maciel, T., 2013, *AJ*, 146, 41
- Schombert, J. M., & McGaugh, S. S., 2014, *PASA*, 31, 11
- Skillman, E. D., Kennicutt, R. C., Hodge, P. W., 1989, *ApJ*, 347, 875
- Skillman, E. D., Terlevich, R., Melnick, J., 1989, *MNRAS*, 240, 563
- Stoughton, C., et al., 2002, *AJ*, 123, 485
- Vacca, W. D., & Conti, P. S., 1992, *ApJ*, 401, 543
- van der Hulst, J. M., Skillman, E. D., Smith, T. R., Bothun, G. D., McGaugh, S. S., de Blok, W. J. G., 1993, *AJ*, 106, 548
- van Zee, L., Haynes, M. P., Salzer, J. J., 1997, *AJ*, 114, 2497
- van Zee, L., 2000, *ApJ*, 119, 2757
- Vorobyov, E. I., Shchekinov, Yu., Bizyaev, D.; Bomans, D., Dettmar, R.-J., 2009, *A&A*, 505, 483
- Werk, J. K., et al., 2008, *ApJ*, 678, 888
- Wen, X.-Q., et al., 2013, *MNRAS*, 433, 2946
- Wright E. L., et al., 2010, *AJ*, 140, 1868
- Wu, H. et al., *ApJ*, 632, 79
- York, D. G., et al., 2000, *AJ*, 120, 1579
- Zackrisson, E.; Bergvall, N.; Östlin, G., 2005, *A&A*, 435, 29
- Zhou, Z-M, Cao, C., Meng, X.-M., Wu, H., 2011, *AJ*, 142, 38
- Zhu, Y.-N., Wu, H., Cao, C., Li, H.-N., 2008, *ApJ*, 686, 155

This paper has been typeset from a \TeX / \LaTeX file prepared by the author.